DOI: 10.1021/ic902484v

Inorganic Chemistry
Article

Synthesis of a Solid Solution Series of Layered $Eu_xGd_{1-x}(OH)_{2.5}Cl_{0.5}\cdot 0.9H_2O$ and Its Transformation into $(Eu_xGd_{1-x})_2O_3$ with Enhanced Photoluminescence Properties

Linfeng Hu,[†,‡] Renzhi Ma,[†] Tadashi C. Ozawa,[†] and Takayoshi Sasaki*[,†,‡]

[†]*International Center for Materials Nanoarchitectonics, National Institute for Materials Science, 1-1 Namiki, Tsukuba, Ibaraki 305-0044, Japan, and* [‡]*Graduate School of Pure and Applied Sciences, University of Tsukuba, 1-1-1 Tennodai, Tsukuba, Ibaraki, 305-8571, Japan*

Received December 15, 2009

The synthesis of a series of new layered rare-earth hydroxide solid solutions and their transformation into $(Eu_xGd_{1-x})_2O_3$ crystallites are described. Highly crystalline platelets of $Eu_xGd_{1-x}(OH)_{2.5}Cl_{0.5}\cdot 0.9H_2O$ solid solutions with various Eu^{3+}/Gd^{3+} ratios were prepared through a homogeneous precipitation method. The hydroxide solid-solution samples exhibited characteristic Eu^{3+} photoluminescence properties through the energy transfer from Gd^{3+} to Eu^{3+} and the self-excitation of Eu^{3+}. Cubic $(Eu_xGd_{1-x})_2O_3$ crystallites were obtained via quasi-topotactic transformation of $Eu_xGd_{1-x}(OH)_{2.5}Cl_{0.5}\cdot 0.9H_2O$ solid solutions above 800 °C. The as-transformed cubic $(Eu_xGd_{1-x})_2O_3$ crystallites well retained the original platelet morphology and single crystalline nature, and exhibited greatly enhanced photoluminescence properties with respect to the precursor hydroxides. The Eu^{3+} content of 0.05 in the cubic $(Eu_xGd_{1-x})_2O_3$ gave a maximum luminescence intensity, which is comparable with that of a commercial Y_2O_3:Eu phosphor.

Introduction

There has been considerable interest in the synthesis of layered inorganic materials because the lamellar structure endows a range of properties that are useful for applications including catalysts, catalyst supports, ion exchangers, sensors, and photofunctional materials.[1] Furthermore, newly developed strategies involving exfoliation of layered materials into nanosheets and reassembly of the resulting nanosheets pave the way to designing novel nanostructures and nanodevices with unique functionalities.[2] A wide variety of layered materials, such as layered metal phosphates,[3] layered transition metal oxides,[4−6] and layered double hydroxides (LDH),[7] have been investigated in the past decades.

Recently, a new family of layered rare-earth hydroxides with a typical composition of $Ln(OH)_{2.5}X_{0.5}\cdot nH_2O$ (Ln = Sm, Eu, Gd, Tb, Dy, Ho, Er, Tm, Yb, Lu, Y; X = interlayer anions) has been synthesized, and has attracted a great deal of interest.[8] Several groups have reported the synthesis and crystal structures of this new layered rare-earth hydroxide family. The compounds of $Ln(OH)_{2.5}X_{0.5}\cdot nH_2O$ (Ln = Gd−Lu, Y; X = Cl^-, NO_3^-, Br^-) were synthesized by a hydrothermal treatment on a precipitate of $LnX_3\cdot mH_2O$ and

*To whom correspondence should be addressed. E-mail: sasaki.takayoshi@nims.go.jp. Fax: (+81) 29-854-9061.

(1) Sideris, P. J.; Nielsen, U. G.; Gan, Z. H.; Grey, C. P. *Science* **2008**, *321*, 113–117.

(2) (a) Osada, M.; Ebina, Y.; Funakubo, H.; Yokoyama, S.; Kiguchi, T.; Takada, K.; Sasaki, T. *Adv. Mater.* **2006**, *18*, 1023–1027. (b) Osada, M.; Ebina, Y.; Takada, K.; Sasaki, T. *Adv. Mater.* **2006**, *18*, 295–299.

(3) (a) Alberti, G.; Casciola, M.; Costantino, U. *J. Colloid Interface Sci.* **1985**, *107*, 256–263. (b) Yamamoto, N.; Okuhara, T.; Nakato, T. *J. Mater. Chem.* **2001**, *11*, 1858–1863.

(4) (a) Sasaki, T.; Watanabe, M.; Hashizume, H.; Yamada, H.; Nakazawa, H. *J. Am. Chem. Soc.* **1996**, *118*, 8329–8335. (b) Sasaki, T.; Watanabe, M. *J. Am. Chem. Soc.* **1998**, *120*, 4682–4689.

(5) (a) Omomo, Y.; Sasaki, T.; Wang, L. Z.; Watanabe, M. *J. Am. Chem. Soc.* **2003**, *125*, 3568–3575. (b) Liu, Z.; Ma, R.; Ebina, Y.; Takada, K.; Sasaki, T. *Chem. Mater.* **2007**, *19*, 6504–6512. (c) Liu, Z.-H.; Ooi, K.; Kanoh, H.; Tang, W. P.; Tomida, T. *Langmuir* **2000**, *16*, 4154–4164. (d) Fukuda, K.; Nakai, I.; Ebina, Y.; Ma, R.; Sasaki, T. *Inorg. Chem.* **2007**, *46*, 4787–4789.

(6) (a) Takagaki, A.; Sugisawa, M.; Lu, D.; Kondo, J. N.; Hara, M.; Domen, K.; Hayashi, S. *J. Am. Chem. Soc.* **2003**, *125*, 5479–5485. (b) Treacy, M. M. J.; Rice, S. B.; Jacobson, A. J.; Lewandowski, J. T. *Chem. Mater.* **1990**, *2*, 279–286.

(7) (a) Ma, R.; Liu, Z.; Takada, K.; Iyi, N.; Bando, Y.; Sasaki, T. *J. Am. Chem. Soc.* **2007**, *129*, 5257–5263. (b) Liu, Z.; Ma, R.; Osada, M.; Iyi, N.; Ebina, Y.; Takada, K.; Sasaki, T. *J. Am. Chem. Soc.* **2006**, *128*, 4872–4880.

(8) (a) McIntyre, L. J.; Jackson, L. K.; Fogg, A. M. *Chem. Mater.* **2008**, *20*, 335–340. (b) Poudret, L.; Prior, T. J.; McIntyre, L. J.; Fogg, A. M. *Chem. Mater.* **2008**, *20*, 7447–7453. (c) Hindocha, S. A.; McIntyre, L. J.; Fogg, A. M. *J. Solid State Chem.* **2009**, *182*, 1070–1074. (d) Lee, K.-H.; Byeon, S.-H. *Eur. J. Inorg. Chem.* **2009**, 929–936. (e) Geng, F.; Xin, H.; Matsushita, Y.; Ma, R.; Tanaka, M.; Izumi, F.; Iyi, N.; Sasaki, T. *Chem.—Eur. J.* **2008**, *14*, 9255–9260. (f) Geng, F.; Matsushita, Y.; Ma, R.; Xin, H.; Tanaka, M.; Izumi, F.; Iyi, N.; Sasaki, T. *J. Am. Chem. Soc.* **2008**, *130*, 16344–16350. (g) Geng, F.; Matsushita, Y.; Ma, R.; Xin, H.; Tanaka, M.; Iyi, N.; Sasaki, T. *Inorg. Chem.* **2009**, *48*, 6724–6730.

Published on Web 02/19/2010

Scheme 1. Schematic Illustration of the Synthesis of $Eu_xGd_{1-x}(OH)_{2.5}Cl_{0.5}\cdot 0.9H_2O$ Solid Solutions and Their Transformation into the Corresponding $(Eu_xGd_{1-x})_2O_3$

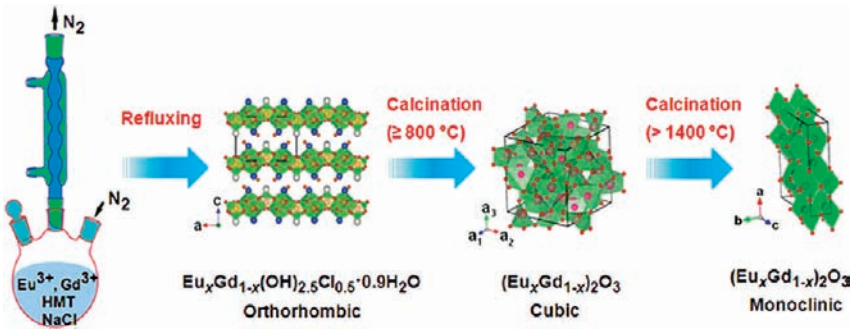

NaOH in the presence of NaX.[8a−c] Thereafter, the members were extended to Sm and Eu by the same hydrothermal method through careful control of pH.[8d] We developed a homogeneous precipitation route utilizing hexamethylenetetramine (HMT) hydrolysis to obtain the well-crystallized $Ln(OH)_{2.5}X_{0.5}\cdot nH_2O$ (Ln = Nd, Sm−Tm, Y; X = Cl^-, NO_3^-).[8e−g] A slow and progressive hydrolysis of HMT makes the solution basic and induces homogeneous precipitation of rare-earth ions. The products mostly exhibit micrometer-sized platelet morphology with a rectangular shape, and crystal-structure analysis has revealed that these new compounds have an orthorhombic layered structure composed of a cationic host layer and charge-compensating anions residing in the interlayer gallery. The lanthanide ions are accommodated in eight- and nine-fold coordination shells consisting of OH^- groups and water molecules. Photoluminescence activators such as Eu^{3+} and Tb^{3+} can be incorporated into these sites of the host layer, exhibiting characteristic red and green emission, respectively.[8e,f] Furthermore, the interlayer anions act as counterions and show ion-exchange reactivities toward a range of anions under ambient conditions.

Rare-earth hydroxide solid solutions, such as $Eu_xGd_{1-x}(OH)_3$, have been studied as precursors for preparing the corresponding rare-earth oxide solid solutions $(Eu_xGd_{1-x})_2O_3$, which exhibit superior photoluminescence properties for various commercial applications such as field emission displays (FED), projection televisions (PTV), and plasma display panels (PDP).[9] However, there has been no report on a solid solution of the new layered rare-earth hydroxides mentioned above. Considering the very close ionic radii of Gd^{3+} (0.1053 nm) and Eu^{3+} (0.1066 nm),[10] these two ions may be able to coprecipitate into this layered structure to form rare-earth hydroxide solid solutions, which would remarkably enrich the layered rare-earth hydroxide family. Furthermore, thermal transformation of these precursor hydroxide solid solutions will result in $(Eu_xGd_{1-x})_2O_3$ solid solutions in a well-developed platelet form, an important red-emitting phosphor because of its high luminescent efficiency and well-defined emission wavelength. On the basis of this concept, we recently doped 0.05 Eu^{3+} to form a $Eu_{0.05}Gd_{0.95}(OH)_{2.5}Cl_{0.5}\cdot 0.9H_2O$ solid solution with uniform platelet morphology. Benefited by their two-dimensional anisotropic morphology, a highly [001] oriented monolayer film of the hydroxide solid solution crystallites was fabricated by a self-assembly method at the hexane/water interface.[11] Since the (001) plane of the rare-earth hydroxide crystal and the (111) plane of the corresponding oxide crystal have a very similar arrangement of rare-earth atoms, a [111] oriented $(Eu_{0.05}Gd_{0.95})_2O_3$ monolayer film was obtained via a quasi-topotactic transformation from the $Eu_{0.05}Gd_{0.95}(OH)_{2.5}Cl_{0.5}\cdot 0.9H_2O$ precursor film. The as-transformed $(Eu_{0.05}Gd_{0.95})_2O_3$ film showed far stronger luminescence intensity than the precursor hydroxide film, and more importantly, more prominent photoluminescence properties than the corresponding oxide powder sample.[12]

The previous study provided a new approach to fabricate a high-quality rare-earth oxide film with excellent photoluminescence properties. To enable these rare-earth compounds to be used as potential commercial phosphor materials, the photoluminescence mechanism and quasi-topotactic transformation process from the hydroxide crystallite to the oxide crystallite must be clarified. We also expect that the photoluminescence properties of $(Eu_xGd_{1-x})_2O_3$ closely depend on the concentration of Eu^{3+} activator. Therefore, comprehensive studies of these layered rare-earth hydroxide solid solutions at various Eu^{3+} contents and their transformation into the corresponding oxides are required to achieve a full understanding of this intriguing series of materials.

In this paper, we present the systematic synthesis of a solid solution series of layered $Eu_xGd_{1-x}(OH)_{2.5}Cl_{0.5}\cdot 0.9H_2O$ with variable Eu^{3+}/Gd^{3+} ratios by the homogeneous precipitation method. Subsequent heat treatment of the $Eu_xGd_{1-x}(OH)_{2.5}Cl_{0.5}\cdot 0.9H_2O$ solid solutions under suitable conditions provided cubic and monoclinic $(Eu_xGd_{1-x})_2O_3$ crystallites (as illustrated in Scheme 1). The quasi-topotactic transformation process and the photoluminescence properties were examined in detail.

Experimental Section

Sample Preparation. In a typical synthetic procedure, $EuCl_3\cdot 6H_2O$ (>99.99%) and $GdCl_3\cdot 6H_2O$ (>99.99%) with a designed molar ratio were dissolved in 1 dm^3 Milli-Q water giving a total concentration of 5 mM. NaCl (65 mmol) and HMT (5 mmol) were then added into this mixture. The mixed solution was heated at the refluxing temperature under magnetic stirring and nitrogen gas protection for 8 h. The product was filtered and washed with water and ethanol several times, and

(9) (a) Wang, X.; Sun, X. M.; Yu, D.; Zou, B. S.; Li, Y. *Adv. Mater.* **2003**, *15*, 1442–1445. (b) Chen, H.; Zhang, J.; Wang, X.; Gao, S.; Zhang, M.; Ma, Y.; Dai, Q.; Li, D.; Kan, S.; Zou, G. *J. Colloid Interface Sci.* **2006**, *297*, 130–133.
(10) Shannon, R. D. *Acta Crystallogr.* **1976**, *A32*, 751–767.
(11) Hu, L.; Ma, R.; Ozawa, T. C.; Geng, F.; Iyi, N.; Sasaki, T. *Chem. Commun.* **2008**, 4897–4899.
(12) Hu, L.; Ma, R.; Ozawa, T. C.; Sasaki, T. *Angew. Chem., Int. Ed.* **2009**, *48*, 3846–3849.

Table 1. Elemental Analysis Results of the As-Prepared Samples

Eu/(Eu+Gd) in starting solutions (molar ratio)		product (mass%) Eu	Gd	OH	Cl	H_2O	C	chemical formula
0.05	Anal.	3.2	64.1	17.5	7.3	6.7	0.2	$Eu_{0.05}Gd_{0.95}(OH)_{2.42}$
	(Calcd.)	(3.25)	(63.94)	(17.61)	(7.29)	(6.63)	(0.26)	$Cl_{0.48}(CO_3)_{0.05}\cdot 0.86H_2O$
0.10	Anal.	6.6	60.3	17.5	7.2	6.9	0.2	$Eu_{0.10}Gd_{0.88}(OH)_{2.38}$
	(Calcd.)	(6.62)	(60.30)	(17.63)	(7.42)	(6.98)	(0.21)	$Cl_{0.48}(CO_3)_{0.04}\cdot 0.89H_2O$
0.30	Anal.	20.2	46.6	17.5	7.3	7.3	0.3	$Eu_{0.30}Gd_{0.68}(OH)_{2.38}$
	(Calcd.)	(19.92)	(46.72)	(17.68)	(7.14)	(7.24)	(0.26)	$Cl_{0.46}(CO_3)_{0.05}\cdot 0.92H_2O$
0.50	Anal.	33.1	33.6	17.7	7.4	7.1	0.2	$Eu_{0.50}Gd_{0.49}(OH)_{2.40}$
	(Calcd.)	(33.03)	(33.50)	(17.74)	(7.56)	(7.12)	(0.21)	$Cl_{0.49}(CO_3)_{0.04}\cdot 0.91H_2O$
0.70	Anal.	46.4	19.8	17.8	7.5	7.3	0.2	$Eu_{0.70}Gd_{0.29}(OH)_{2.40}$
	(Calcd)	(46.39)	(19.89)	(17.79)	(7.59)	(7.30)	(0.21)	$Cl_{0.49}(CO_3)_{0.04}\cdot 0.93H_2O$
0.90	Anal.	60.0	6.4	17.8	7.5	7.2	0.2	$Eu_{0.90}Gd_{0.09}(OH)_{2.40}$
	(Calcd.)	(60.01)	(6.21)	(17.90)	(7.64)	(7.19)	(0.21)	$Cl_{0.49}(CO_3)_{0.04}\cdot 0.91H_2O$

finally dried at room temperature at a controlled humidity of 70%. To obtain the $(Eu_xGd_{1-x})_2O_3$ oxide solid solution, the corresponding hydroxide samples were calcined at 800−1500 °C for 2 h in air.

Sample Characterization. The phase purity and evolution were examined by powder X-ray diffraction (XRD) using a Rigaku RINT-2000 diffractometer with Cu Kα radiation. The contents of Eu and Gd in the sample were determined by inductively coupled plasma atomic emission spectrophotometry (Seiko SPS1700HVR instrument) after the sample was dissolved in an aqueous HCl solution. OH content was obtained by back-titration with 0.1 M standard Na_2CO_3 after dissolving the sample in 0.1 M standard H_2SO_4. Cl content was quantified by an LC-8020 ion chromatography system. Carbon and water contents were measured on a LECO RC-412 C, H_2O-analyzer. Scanning electron microscopy (SEM) images were taken with a Keyence VE8800 microscope at an accelerating voltage of 10 kV. Transmission electron microscopy (TEM) images and selected area electron diffraction (SAED) patterns were obtained on a JEOL JEM-3100F energy-filtering (Omega type) transmission microscope. The photoluminescence excitation and emission spectra were measured on a Hitachi F-7000 fluorescence spectrophotometer at room temperature using 700 and 400 V for the hydroxide and oxide samples, respectively. Thermogravimetry-differential thermal analysis (TG-DTA) measurements were carried out using a Rigaku TGA-8120 instrument in a temperature range of 25−1000 °C at a heating rate of 5 °C min^{-1} under air flow.

Results and Discussion

Synthesis and Characterization of $Eu_xGd_{1-x}(OH)_{2.5}Cl_{0.5}\cdot 0.9H_2O$ Solid Solutions. The homogeneous precipitation method was successfully used to prepare Eu−Gd hydroxide solid solutions. The starting solutions became turbid, yielding white precipitates after 1 h of the reaction. Table 1 shows chemical analysis results of the products after a refluxing process for 8 h. As can be seen, the Eu^{3+}/Gd^{3+} molar ratios of all samples were consistent with those in the starting mixed solutions of Eu and Gd chlorides, revealing that quantitative coprecipitation of Eu^{3+} and Gd^{3+} was achieved. Applying the rational charge balancing, the chemical compositions of all products can be expressed by a general formula of $Eu_xGd_{1-x}(OH)_{2.5}Cl_{0.5}\cdot 0.9H_2O$, which is consistent with the previous report on rare-earth hydroxides.[8e]

Figure 1a shows powder XRD patterns of selected samples with Eu^{3+} compositions at 0, 0.3, 0.5, 0.8, and 1.0. All the diffraction peaks can be indexed based on the orthorhombic structure of layered rare-earth hydroxides

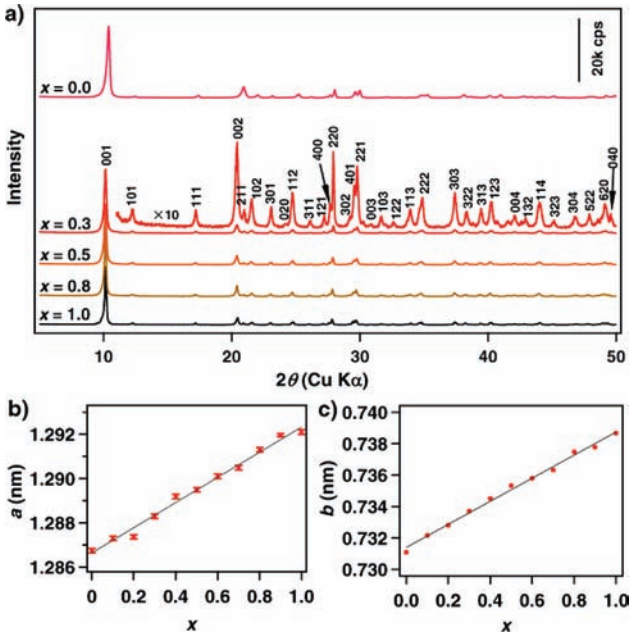

Figure 1. (a) XRD patterns of the as-prepared $Eu_xGd_{1-x}(OH)_{2.5}Cl_{0.5}\cdot 0.9H_2O$ samples (x = 0, 0.3, 0.5, 0.8, 1.0). The enlarged view of the pattern in the 2θ range of 11−50° is shown for the sample of x = 0.3. (b, c) Lattice parameters, a and b, as a function of Eu^{3+} content (the standard deviations for the parameter b are smaller than the sizes of the markers).

reported in our previous study.[8e] The 001 reflection of the samples with Eu^{3+} content from 0.1 to 0.9 was located at nearly the same 2θ angle of 10.2°, indicating a basal spacing of 0.86 nm. The basal spacing for the samples with Eu^{3+} contents lower than 0.1 decreased to 0.84 nm (see Figure S1 in the Supporting Information), reflecting the distinct hydration behavior of the compound series.[13] The general *hkl* reflections were sharp (inset of Figure1a),

(13) The layered rare-earth hydroxides of $Ln(OH)_{2.5}X_{0.5}\cdot nH_2O$ (Ln=Sm, Eu, Gd) display a high- hydration (HH) at a high relative humidity (RH) and low-hydration (LH) phase at a low RH. The interlayer spacing for the HH and LH phases are 0.85−0.86 and 0.83−0.84 nm, respectively. For Eu end phase, the HH phase undergoes transformation into the LH phase at a critical RH of 20%, which is lower than that of the Gd phase (at a critical RH of 50%).[8f] Because XRD patterns of the present layered hydroxide solid solutions were measured at an ambient environment (RH about 30−40%), the samples at high Eu^{3+} content showed the similar hydration state with that of the HH phase, corresponding to a larger interlayer spacing of 0.86 nm. The samples at low Eu^{3+} content exhibited a smaller spacing of 0.84 nm, agreeing with that of the LH phase.

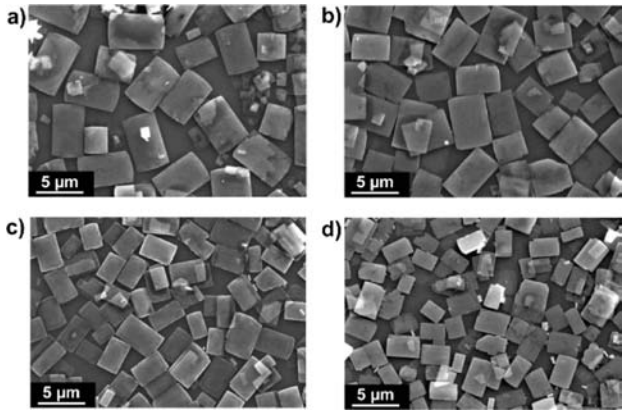

Figure 2. Typical SEM images of $Eu_xGd_{1-x}(OH)_{2.5}Cl_{0.5}\cdot 0.9H_2O$ solid solutions: (a) $x = 0.2$, (b) 0.6, (c) 0.8, and (d) 0.9.

indicating the high crystallinity of the products. The refined lattice parameters *a* and *b* along the intralayer are plotted as a function of Eu^{3+} content (Figure 1b, c). Because of the larger ionic radius for Eu^{3+} than Gd^{3+}, the *a* and *b* parameters increased as the Eu^{3+} content increased, and the trend was almost linear, following the Vegard's law.[14] This result provides essential evidence that Eu^{3+} and Gd^{3+} are successfully incorporated into the host lattice to form layered hydroxide solid solutions. The Eu^{3+} content in the host layer can be adjusted as required from 0 to 1 to yield samples with controllable compositions.

Typical SEM images of the $Eu_xGd_{1-x}(OH)_{2.5}Cl_{0.5}\cdot 0.9H_2O$ solid solution crystallites are shown in Figures 2 and S2 (Supporting Information). All of the hydroxide solid solution samples displayed rectangular platelet morphology with flat surfaces and sharp corners, indicating that they were well crystallized. The average size of $Eu_{0.2}Gd_{0.8}(OH)_{2.5}Cl_{0.5}\cdot 0.9H_2O$ is about $4 \times 2\ \mu m^2$, and it tends to become smaller as the Eu^{3+} content increases. A similar tendency was also observed in the wet-process synthesis of $(Gd_xY_{1-x})_2O_3$ ($x = 0-1.0$) solid solutions[15] and might be attributed to the higher nucleation rate of Eu^{3+} than Gd^{3+} in the present homogeneous precipitation system resulting from the lanthanide contraction phenomenon.[16] In general, a slow nucleation rate is favorable for the growth of large crystals. Therefore, the hydroxide solid solution platelets displayed smaller size for Eu^{3+}-rich phases.

Photoluminescence Properties of $Eu_xGd_{1-x}(OH)_{2.5}Cl_{0.5}\cdot 0.9H_2O$ Solid Solutions. Photoluminescence properties of $Eu_xGd_{1-x}(OH)_{2.5}Cl_{0.5}\cdot 0.9H_2O$ solid solutions are depicted in Figures 3 and 4. The excitation spectrum of the Eu-end phase consists of a series of sharp peaks attributable to the intra $4f^6$ transitions of Eu^{3+} (Figure 3a). For the hydroxide solid solution samples, additional excitation peaks were observed at 245−250, 273, 305−312 nm, which can be assigned to the transitions from the ground level $^8S_{7/2}$ to excited levels ^6D_J, ^6I_J, and ^6P_J of Gd^{3+}, respectively.[17] Upon excitation of the $^8S_{7/2}$-^6I_J transition

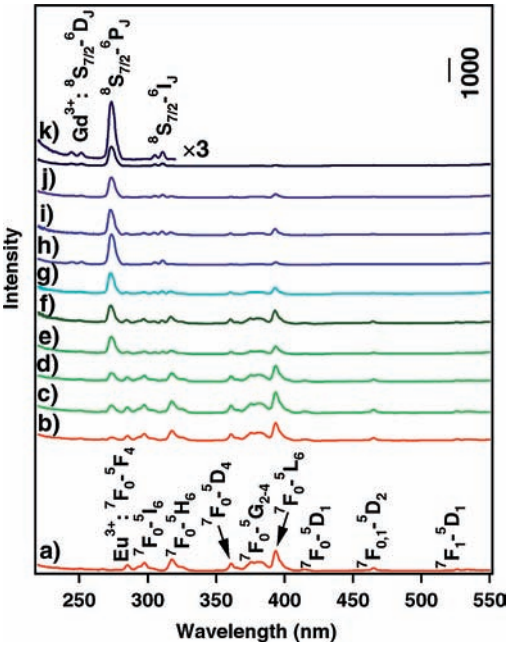

Figure 3. Room-temperature excitation spectra of $Eu_xGd_{1-x}(OH)_{2.5}Cl_{0.5}\cdot 0.9H_2O$ solid solutions monitored at 615 nm: (a) $x = 1.0$, (b) 0.8, (c) 0.6, (d) 0.4, (e) 0.2, (f) 0.1, (g) 0.07, (h) 0.05, (i) 0.03, (j) 0.01, and (k) 0.005.

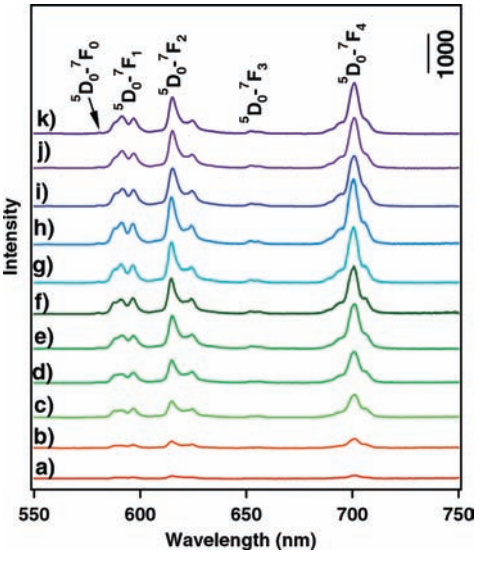

Figure 4. Room-temperature emission spectra of $Eu_xGd_{1-x}(OH)_{2.5}Cl_{0.5}\cdot 0.9H_2O$ solid solutions excited at 273 nm: (a) $x = 1.0$, (b) 0.8, (c) 0.6, (d) 0.4, (e) 0.2, (f) 0.1, (g) 0.07, (h) 0.05, (i) 0.03, (j) 0.01, and (k) 0.005.

of Gd^{3+}, all samples exhibited typical photoluminescence peaks at 579, 595, 615, 651, and 701 nm, because of $^5D_0-^7F_J$ ($J = 0-4$) radiative-relaxational transition of Eu^{3+} (Figure 4). The presence of Eu^{3+} emissions through the excitation of Gd^{3+} transitions indicates efficient energy transfer from Gd^{3+} to Eu^{3+}, suggesting that there is a strong interaction between these two ions in the host hydroxide layer. The possible energy transfer mechanism is illustrated in Figure S3 (Supporting Information).[17] When the samples are excited by UV-lamp, the energy absorbed by the samples induces the electronic transition from the Gd^{3+} ground level $^8S_{7/2}$ to the excited levels ^6D_J,

(14) Yuan, Q.; Liu, Q.; Song, W.-G.; Feng, W.; Pu, W.-L.; Sun, L.-D.; Zhang, Y.-W.; Yan, C.-H. *J. Am. Chem. Soc.* **2007**, *129*, 6698–6699.
(15) Li, J.-G.; Li, X.; Sun, X.; Ikegami, T.; Ishigaki, T. *Chem. Mater.* **2008**, *20*, 2274–2281.
(16) Krumholz, P. *Progress in the Science and Technology of the Rare Earths*; Eyring, L., Ed.; Pergamon Press: New York, 1964.
(17) Li, Y.-C.; Chang, Y.-H.; Chang, Y.-S.; Lin, Y.-J.; Laing, C.-H. *J. Phys. Chem. C* **2007**, *111*, 10682–10688.

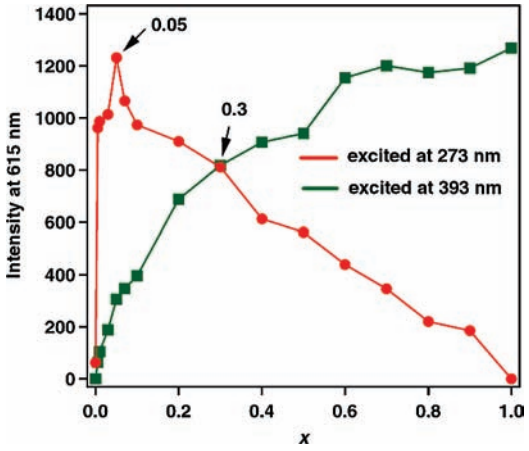

Figure 5. Emission intensity at 615 nm as a function of Eu^{3+} content excited at 273 and 393 nm, respectively.

^6I_J, and ^6P_J. Some of the electrons in the excited levels of Gd^{3+} transfer to the $^5D_0$ level of Eu^{3+} and then to the ^5F_J ($J = 0-4$) levels of Eu^{3+}, yielding the Eu^{3+} emissions.

Figure 5 shows the emission intensity of the hydroxide solid solutions as a function of the Eu^{3+} content excited by the energy transfer from Gd^{3+} to Eu^{3+} (at 273 nm) and Eu^{3+} 4f−4f transitions (at 393 nm). For the emission through the energy transfer from Gd^{3+} to Eu^{3+}, the intensity increased sharply as the Eu^{3+} content increased until it reached the optimal content of 0.05. A further increase in the Eu^{3+} content, in turn, led to a steady decrease in the luminescence intensity. This phenomenon is thought to be caused by the decrease in effective absorption cross section of Gd^{3+} with higher Eu^{3+} content in the hydroxide solid solution samples. Moreover, a concentration quenching effect may also contribute to the decrease in emission intensity.[18] As is well-known, when the Eu^{3+} content in the hydroxide host layer is too high, the higher probability of energy transfer among the Eu^{3+} activators themselves results in the decrease of luminescence intensity. The emission intensity through the direct excitation of Eu^{3+} transition at 393 nm increased progressively with the increase in Eu^{3+} content (see Figure S4 in the Supporting Information). This behavior is attributed to the increased number of emission centers and absorption cross section of Eu^{3+}, and suggests that the emission through the direct Eu^{3+} excitation was the more prominent relaxation process than the nonradiative relaxation process through the concentration quenching effect. The emission through the excited energy transfer from Gd^{3+} to Eu^{3+} was nearly equal in intensity to that through the direct Eu^{3+} excitation when the Eu^{3+} content was 0.3.

$(Eu_xGd_{1-x})_2O_3$ Crystallites: Quasi-Topotactic Transformation from $Eu_xGd_{1-x}(OH)_{2.5}Cl_{0.5}\cdot 0.9H_2O$ Solid Solutions. The layered $Eu_xGd_{1-x}(OH)_{2.5}Cl_{0.5}\cdot 0.9H_2O$ solid solutions were readily converted into $(Eu_xGd_{1-x})_2O_3$ upon annealing. The phase evolution from the precursor hydroxide to oxide was examined at various calcination temperatures. As can be clearly seen in Figure 6 for the $Eu_{0.05}Gd_{0.95}(OH)_{2.5}Cl_{0.5}\cdot 0.9H_2O$ sample

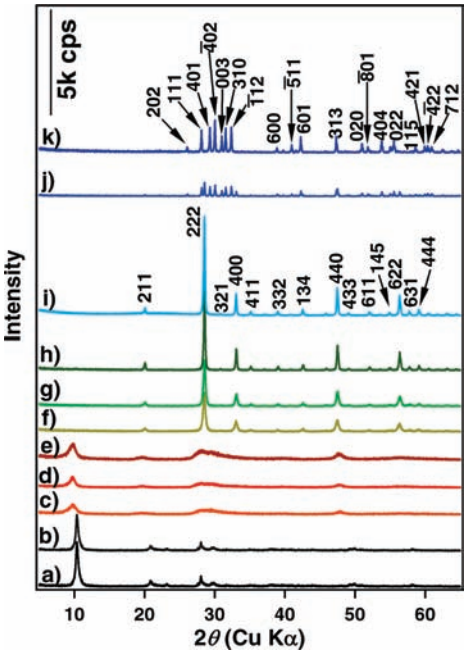

Figure 6. Powder XRD patterns of $Eu_{0.05}Gd_{0.95}(OH)_{2.5}Cl_{0.5}\cdot 0.9H_2O$ solid solution as a function of the calcination temperature showing the phase evolution: (a) precursor, (b) 100, (c) 300, (d) 500, (e) 700, (f) 800, (g) 1000, (h) 1200, (i) 1300, (j) 1400, and (k) 1500 °C.

as an example, the XRD pattern of the product calcined at 100 °C for 2 h showed negligible changes from the pristine phase except for a decrease in intensity. The products calcined at 300−700 °C only exhibited the 00*l* reflections with much lower intensities. These results may be ascribed to the well-known "reconstruction phenomenon" or "memory effect" of LDHs.[19] The layered structure of the hydroxide solid solutions might collapse at these calcination temperatures and be recovered by the adsorption of water in air during the cooling process. The reconstruction behavior of the rare-earth hydroxides is underway, and the details will be described elsewhere. Pure cubic $(Eu_{0.05}Gd_{0.95})_2O_3$ (space group: *Ia3*) phase was evolved at 800 °C. The corresponding XRD pattern is obviously different from that of the oriented $(Eu_{0.05}Gd_{0.95})_2O_3$ monolayer film prepared from a self-assembled hydroxide crystallite film under the same annealing conditions in our previous study.[12] In contrast to the powder sample, only 222 and 444 reflections were detected for the as-transformed $(Eu_{0.05}Gd_{0.95})_2O_3$ film, indicating that it was highly oriented along the [111] direction of the crystallites. Because the [111] oriented oxide film was thermally transformed from the [001] oriented hydroxide film, it is likely that the (001) plane of the hydroxide precursor developed into the (111) plane of $(Eu_{0.05}Gd_{0.95})_2O_3$ during the transformation. We have previously pointed out that the (001) plane of $Eu_{0.05}Gd_{0.95}(OH)_{2.5}Cl_{0.5}\cdot 0.9H_2O$ precursor and the (111) plane of $(Eu_{0.05}Gd_{0.95})_2O_3$ are very similar in terms of the arrangement of rare-earth atoms.[12] Therefore, the rare-earth atoms in the hydroxide precursor can retain their initial structural arrangement after the simultaneous evaporation of water molecules and decomposition of OH^- groups to form the oxide crystal. This process can be

(18) (a) Blasse, G. *Philips Res. Rep.* **1969**, *24*, 131–144. (b) Yuan, J.-L.; Zeng, X.-Y.; Zhao, J.-T.; Zhang, Z.-J.; Chen, H.-H.; Zhang, G.-B. *J. Solid State Chem.* **2007**, *180*, 3310–3316.

(19) Vera, R. L. C.; Thomas, J. P. *Inorg. Chem.* **1995**, *34*, 883–892.

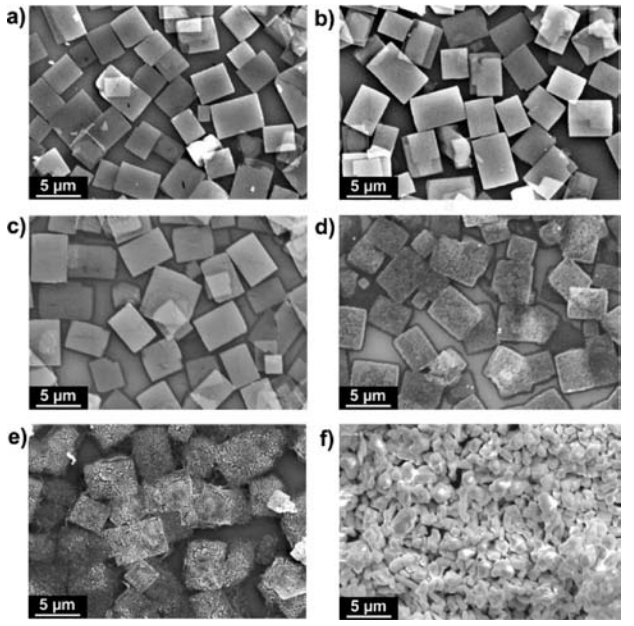

Figure 7. Typical SEM images of (a) $Eu_{0.05}Gd_{0.95}(OH)_{2.5}Cl_{0.5}\cdot 0.9H_2O$ precursor and as-transformed crystallites at (b) 400, (c) 800, (d) 1000, (e) 1200, and (f) 1400 °C.

called "quasi-topotactic transformation".[20] The process of phase evolution was also confirmed by TG-DTA. As shown in Figure S5 (Supporting Information), the weight loss of the sample ended at 850 °C, consistent with the oxide formation at this temperature on the basis of XRD data. When the temperature was further increased to 1200 °C, the diffraction intensity increased apparently and the peaks became sharper, indicating that the crystallinity improved at higher temperature. It is reported that the cubic Gd_2O_3 phase converts to the monoclinic phase (space group: $C2/m$) at 1250 °C.[21] In the present study, the monoclinic phase appeared above 1400 °C.

Figure 7 shows typical SEM images of the $Eu_{0.05}Gd_{0.95}(OH)_{2.5}Cl_{0.5}\cdot 0.9H_2O$ precursor and the as-transformed crystallites at various temperatures. Compared with the precursor hydroxide, the crystallites calcined at 400 °C exhibited no apparent morphological modification (Figure 7a, b). At the temperature of 800 °C when the phase transformation into the cubic phase was completed, the rectangular platelet morphology was still well retained (Figure 7c), probably because of the uniform nucleation and growth of $(Eu_{0.05}Gd_{0.95})_2O_3$ via the quasi-topotactic transformation. The platelets obtained at 1000 °C exhibited rough surfaces with some pores (Figure 7d). When the calcination temperature was increased up to 1200 °C, the roughness and cracks became more apparent (Figure 7e). The sample annealed at 1400 °C showed irregular morphology with average size of about 2−3 μm (Figure 7f). The loss of the platelet morphology at this temperature is ascribed to the phase transformation from cubic to monoclinic $(Eu_{0.05}Gd_{0.95})_2O_3$.

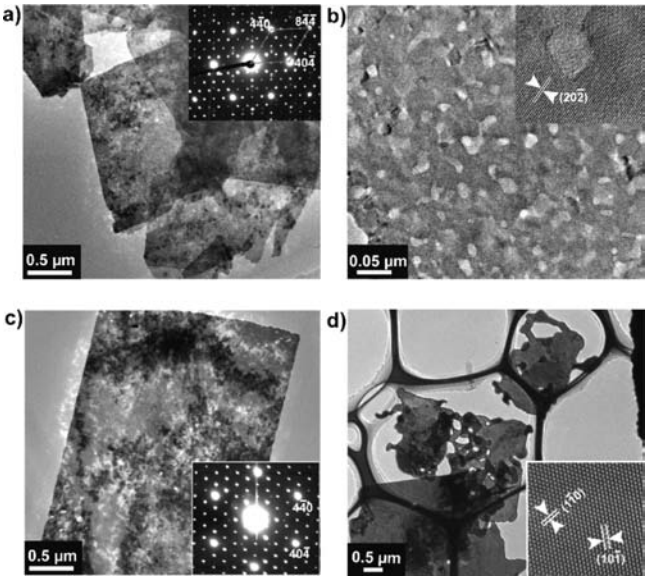

Figure 8. Typical TEM images of cubic $(Eu_{0.05}Gd_{0.95})_2O_3$ platelets transformed at (a) 800, (c) 1000, and (d) 1200 °C, respectively. (b) The nanopores on the surface of the $(Eu_{0.05}Gd_{0.95})_2O_3$ platelets transformed at 800 °C. Insets of (a) and (c) are the SAED patterns taken from individual platelet transformed at 800 and 1000 °C, respectively. Insets of (b) and (d) show the HRTEM images of the corresponding platelet surface.

The results of TEM observation are comparable to those of SEM characterization. The platelet morphology for the sample transformed at 800 °C was further confirmed as shown in Figure 8a. However, close observation at high magnification (Figure 8b) revealed the presence of abundant nanopores with the size of 10−20 nm on the surface. The formation of the pores can be attributed to the volume shrinkage during the transformation. The lattice parameters for the orthorhombic precursor hydroxide are $a = 1.2871$, $b = 0.7316$, and $c = 0.8502$ nm, while that for the as-transformed cubic oxide is $a = 1.0817$ nm. Since each unit-cell of $Eu_{0.05}Gd_{0.95}(OH)_{2.5}Cl_{0.5}\cdot 0.9H_2O$ and $(Eu_{0.05}Gd_{0.95})_2O_3$ contains 8 and 32 rare-earth atoms, respectively, a volume ratio for the same number of rare-earth atoms is defined as follows:

$$R = (V_{\text{oxide}}/4V_{\text{hydroxide}}) \times 100\%$$

where $V_{\text{hydroxide}}$ and V_{oxide} are the unit-cell volumes of $Eu_{0.05}Gd_{0.95}(OH)_{2.5}Cl_{0.5}\cdot 0.9H_2O$ crystal ($= 1.2871 \times 0.7316 \times 0.8502$ nm^3) and $(Eu_{0.05}Gd_{0.95})_2O_3$ crystal ($= 1.0817^3$ nm^3), respectively. The estimated volume ratio is 39.5%, meaning that the volume shrinkage in the transformation process was significant. Such large volume change can be ascribed to the collapse of the layered structure involving the evaporation of water molecules and decomposition of OH^- groups, and it is compensated by the formation of nanopores in the as-transformed oxide platelets, retaining the original platelet shape and size. The TEM image of the platelets annealed at 1000 °C shows much rougher surface than that at 800 °C (Figure 8c). Pores on the surface grew in size as their number decreased. When the temperature was raised to 1200 °C, many cracks appeared on the surface of platelets (Figure 8d), consistent with the SEM image

(20) (a) Yu, C. C.; Zhang, L. X.; Shi, J. L.; Zhao, J. J.; Gao, J. H.; Yan, D. S. *Adv. Funct. Mater.* **2008**, *18*, 1544–1554. (b) Zheng, J.; Jiang, Z.-Y.; Kuang, Q.; Xie, Z.-X.; Huang, R.-B.; Zheng, L.-S. *J. Solid State Chem.* **2009**, *182*, 115–121. (c) Li, L.; Sun, N.; Huang, Y.; Qin, Y.; Zhao, N.; Gao, J.; Li, M.; Zhou, H.; Qi, L. *Adv. Funct. Mater.* **2008**, *18*, 1194–1201.

(21) Jacobsohn, L. G.; Bennett, B. L.; Muenchausen, R. E.; Tornga, S. C.; Thompson, J. D.; Ugurlu, O.; Cooke, D. W.; Sharma, A. L. L. *J. Appl. Phys.* **2008**, *103*, 104303.

(Figure 7e). However, domains surrounded by the cracks displayed smooth surfaces with homogeneous contrast, and the corresponding XRD pattern showed much sharper diffraction peaks than that transformed at the lower temperature of 800 °C (Figure 6). This characteristic implies that $(Eu_{0.05}Gd_{0.95})_2O_3$ recrystallized at 1200 °C.

The SAED patterns taken from an individual platelet transformed at 800 and 1000 °C showed hexagonally arranged sharp diffraction spots which can be indexed to the [111] zone axis pattern (insets of Figure 8a, c). The appearance of forbidden diffraction spots of $10\bar{1}$ and $1\bar{1}0$ for the space group *Ia*3 can be attributed to multiple reflection effects in the $(Eu_{0.05}Gd_{0.95})_2O_3$ platelets. Since the platelets generally lay flat on the copper grid perpendicular to the electron beam, the observed diffraction spots of the [111] zone axis indicate that each $(Eu_{0.05}Gd_{0.95})_2O_3$ platelet is a single crystal with the top (111) surface. The present SAED results again support the quasi-topotactic transformation in which the (111) plane of $(Eu_{0.05}Gd_{0.95})_2O_3$ evolved from the (001) plane of the precursor hydroxide.

High-resolution TEM (HRTEM) images further support the quasi-topotactic transformation as shown in the insets of Figure 8b and d. For the platelets obtained at 800 °C, the lattice fringe was clearly observed, and at a spacing that corresponded closely to the {202} planes of the cubic $(Eu_{0.05}Gd_{0.95})_2O_3$ (inset of Figure 8b). Although the surface was rough and porous, lattice fringes can be seen running long distances, also confirming the single crystalline nature of the whole platelet. When the temperature was increased to 1200 °C, the corresponding HRTEM image exhibited a clear two-dimensional lattice fringe (inset of Figure 8d), demonstrating the significant improvement of crystallinity, which is consistent with the sharp diffraction peaks in the corresponding XRD data (Figure 6). The 0.76 nm spacing of the lattice fringes agrees well with the expected separation of {101} planes.

The formation of the nanopores and quasi-topotactic transformation to oxide appeared to be contradictory at first glance. The abundant pores on the as-transformed $(Eu_{0.05}Gd_{0.95})_2O_3$ platelets and the large shrinkage of lattice volume from hydroxide to oxide suggest a long-distance migration of the rare-earth atoms in the precursor crystal. Thus, it is surprising that the single crystalline nature of the platelets remained after the transformation. This phenomenon can be understood in terms of a mosaic structure.[22] During the transformation from the hydroxide to the oxide platelet, a large number of small crystalline domains may form inside the hydroxide platelet. In each small crystalline domain, the hydroxide structure is converted into the oxide via the quasi-topotactic pathway. The boundaries between these small domains may gradually grow into the as-observed nanopores because of the large volume shrinkage. However, the small domains retain their good crystallographic alignment with each other. Therefore, the whole $(Eu_{0.05}Gd_{0.95})_2O_3$ platelet retains a single-crystal nature. Kobayashi et al. reported a similar quasi-topotactic transformation from Ni−Co−Al LDH platelet to the corresponding spinel platelet.[22] The process should be similar to the present case involving the evolution of small domains or mosaic structure. Note that the as-obtained $(Eu_{0.05}Gd_{0.95})_2O_3$ exhibited much sharper diffraction peaks than Ni−Co−Al spinel, suggesting that the degree of orientation misalignment in the $(Eu_{0.05}Gd_{0.95})_2O_3$ platelet was much smaller than that in the Ni−Co−Al spinel platelet.

All the results demonstrate that rectangular $(Eu_{0.05}Gd_{0.95})_2O_3$ platelets could be obtained by the thermal transformation from the layered hydroxide solid solutions at 800−1200 °C. Although $(Eu_xGd_{1-x})_2O_3$ nanoparticles, nanorods, and colloidal spheres have been widely synthesized in the past,[23] there have been few reports on the preparation of $(Eu_xGd_{1-x})_2O_3$ platelet crystallites. Recently, micrometer-sized $(Eu_xGd_{1-x})_2O_3$ platelets were synthesized through a solution-based method from a pulp precursor. However, the products contained some impurities such as $Gd(OH)_3$.[24] In the present study, we developed a feasible way to obtain uniform $(Eu_xGd_{1-x})_2O_3$ platelets with high purity and crystallinity. This platelet product is a useful building block for fabricating oriented $(Eu_xGd_{1-x})_2O_3$ films, which show superior luminescence properties compared with randomly oriented crystallites in powder samples.[12]

Photoluminescence Properties of the As-Transformed $(Eu_xGd_{1-x})_2O_3$. Figure 9 depicts the room-temperature photoluminescence spectra of cubic $(Eu_xGd_{1-x})_2O_3$ transformed at 1000 °C with varying Eu^{3+} contents in the 0.01−0.3 range. The excitation spectra of all the samples consist of two broad intense bands with their maxima at 224 and 248 nm, which are attributed to the Gd_2O_3 host excitation band and the charge transfer band (CTB) of the electrons between the 2p orbital of O^{2-} and 4f orbital of Eu^{3+}, respectively.[25] The emission through the latter exhibited a higher intensity than the former. In addition, the excitations of the $Gd^{3+8}S_{7/2}$-^6I_J transition at 273 nm, superimposed on the broad CTB peak, and the $Gd^{3+8}S_{7/2}$-^6P_J transition at 313 nm were detected. Therefore, there exist three kinds of energy transfer pathways to Eu^{3+} from the Gd_2O_3 host, CTB and Gd^{3+}, and the observed emissions were dominated by the former two. On the other hand, the general excitation f-f transition lines of Eu^{3+} in the longer wavelength region were relatively weak. In the emission spectra, all the emission lines at 582, 589−601, 613, 654, and 709 nm are characteristic of $^5D_0-^7F_J$ ($J = 0, 1, 2, 3, 4$) transitions of Eu^{3+}, respectively. It is known that relative emission intensities from these intra-Eu^{3+} transitions are sensitive to the local Eu^{3+} environment such as coordination and crystal fields. The highest emission intensity was observed at 613 nm for the electric dipole $^5D_0-^7F_2$ transition, indicating that Eu^{3+} is accommodated in a site with no inversion symmetry.[26] The significant dependence of luminescence intensity on the Eu^{3+} activator content is demonstrated in the inset of Figure 9. The emission intensity exhibited the

(22) Kobayashi, Y.; Ke, X.; Hata, H.; Schiffer, P.; Mallouk, T. E. *Chem. Mater*. **2008**, *20*, 2374–2381.

(23) (a) Mahajan, S. V.; Dickerson, J. H. *Nanotechnology* **2007**, *18*, 325605. (b) Yang, J.; Li, C.; Cheng, Z.; Zhang, X.; Quan, Z.; Zhang, C.; Lin, J. *J. Phys. Chem. C* **2007**, *111*, 18148–18154. (c) Li, J.-G.; Li, X.; Sun, X.; Ishigaki, T. *J. Phys. Chem. C* **2008**, *112*, 11707–11716.

(24) Park, J. K.; Kim, K. N.; Bae, P. K.; Lee, J. H.; Han, C. H.; Kim, C. H. *Electrochem. Solid State Lett*. **2007**, *10*, J97–J100.

(25) Pang, M. L.; Lin, J.; Fu, J.; Xing, R. B.; Luo, C. X.; Han, Y. C. *Opt. Mater*. **2003**, *23*, 547–558.

(26) Antic-Fidancev, E.; Hölsä, J.; Lastusaari, M. *J. Alloys Compd*. **2002**, *341*, 82–86.

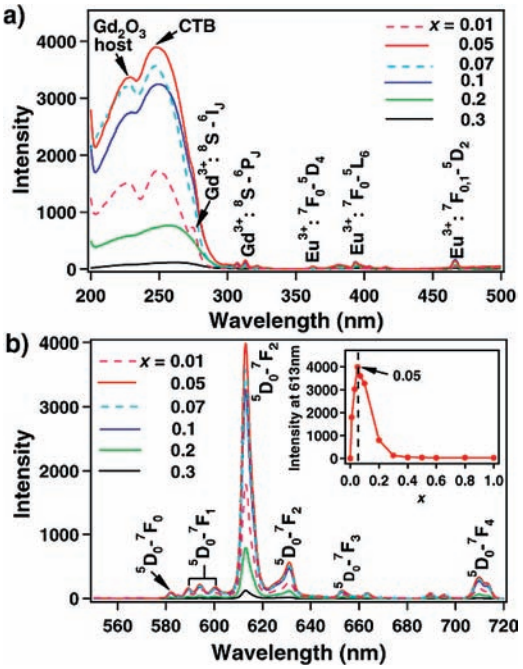

Figure 9. (a) Excitation spectra monitored at 613 nm and (b) emission spectra excited at 248 nm of $(Eu_xGd_{1-x})_2O_3$ (x = 0.01, 0.05, 0.07, 0.1, 0.2, 0.3) transformed at 1000 °C for 2 h. Inset is the emission maxima of the as-transformed $(Eu_xGd_{1-x})_2O_3$ at 1000 °C as a function of the Eu^{3+} content.

maximum when the Eu^{3+} activator content was 0.05 and decreased significantly with increasing Eu^{3+} content above this value, which might be due to the concentration quenching effect.

Keeping Eu^{3+} at the optimal content of 0.05, the effect of calcination temperature on the photoluminescence properties was examined as shown in Figure 10. The luminescence intensity of the resultant $(Eu_{0.05}Gd_{0.95})_2O_3$ remarkably depended on the calcination temperature. The precursor hydroxide exhibited very weak emission. Calcination in the range of 200−600 °C made no apparent difference to the photoluminescence properties, suggesting that the products at this temperature range were not the oxide but the reconstructed structure of the precursor hydroxides. A drastic increase in the intensity was observed above 800 °C, corresponding to the formation of cubic $(Eu_{0.05}Gd_{0.95})_2O_3$ phase. This increase is ascribed to the thorough removal of OH^- groups and water molecules in the layered hydroxide solid-solution crystal, which involve nonradiative energy transfer to OH^- vibration and thus decrease the probability of radiative transitions. The emission intensity increased for the film samples annealed at 800−1000 °C. This increase in the intensity should be due to the improved crystallinity of the products, which is consistent with the XRD data in Figure 6. Further increase of the temperature up to 1200 °C deteriorated the luminescence intensity; the reason may be attributed to the porous and rough surface of the platelets, which seriously affected the luminescence intensity through various factors such as reflection of incident light. The spectral profile of the product calcined at 1500 °C showed a marked change due to the phase transformation from the cubic into the monoclinic $(Eu_{0.05}Gd_{0.95})_2O_3$. The excitation spectrum of the monoclinic phase was virtually identical in profile

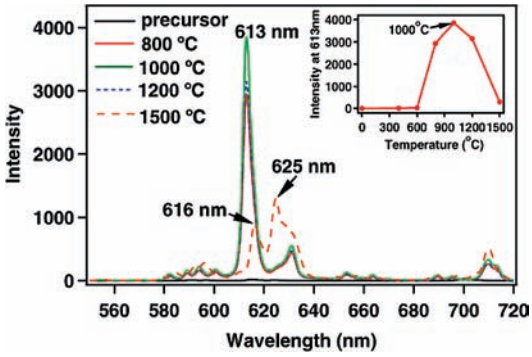

Figure 10. Emission spectra of $Eu_{0.05}Gd_{0.95}(OH)_{2.5}Cl_{0.5}\cdot 0.9H_2O$ precursor (excited at 273 nm), the cubic and monoclinic $(Eu_{0.05}Gd_{0.95})_2O_3$ (excited at 248 nm). Inset is the emission intensity at 613 nm of the as-transformed $(Eu_{0.05}Gd_{0.95})_2O_3$ as a function of calcination temperature.

but lower in intensity compared with that of the cubic phase (see Figure S6 in the Supporting Information), which is consistent with the previous study.[27] For the emission spectra, the peak of Eu^{3+} $^5D_0-^7F_2$ transition exhibited a shift in peak-top position from 613 nm (cubic) to 616 nm (monoclinic), which may be due to the different relative intensities of its five Stark components. Such a difference could arise from the existence of oxygen vacancies in the monoclinic phase and different chemical environment in these two structures.[28] Moreover, an additional peak at 625 nm appeared and exhibited the highest emission intensity. This peak arose from the splitting of the Eu^{3+} $^5D_0-^7F_2$ transition peak, which is a typical feature for Eu^{3+} emission in the monoclinic structure of lanthanide oxides.[29] The relationship between emission intensity of the products and calcination temperature is plotted in the inset of Figure 10. As can be seen, the cubic $(Eu_{0.05}Gd_{0.95})_2O_3$ transformed at 1000 °C exhibited the maximum luminescence intensity, which is comparable with that of a commercially available Y_2O_3:Eu phosphor powder (Kasei Optonix Ltd., see Figure S7 in the Supporting Information). The excellent performance of $(Eu_{0.05}Gd_{0.95})_2O_3$ in the present study is mainly due to its high purity, good crystallinity, high packing density because of the platelet morphology, and uniform distribution of Eu^{3+} activators in the oxide platelets. All of these are advantageous features for quasi-topotactic transformation from the rare-earth hydroxide solid solution platelets to the corresponding oxides.

Conclusions

We have synthesized a new family of $Eu_xGd_{1-x}(OH)_{2.5}Cl_{0.5}\cdot 0.9H_2O$ solid solutions with uniform platelet morphology by a homogeneous precipitation route. The Eu^{3+}/Gd^{3+} ratios in the hydroxide solid solution samples were varied simply by controlling the Eu^{3+}/Gd^{3+} ratio in the starting solution. The hydroxide solid-solution samples

(27) (a) Ozawa, T. C.; Fukuda, K.; Akatsuka, K.; Ebina, Y.; Sasaki, T. *Chem. Mater.* **2007**, *19*, 6575–6580. (b) Kang, Y. C.; Park, S. B.; Lenggoro, I. W.; Okuyama, K. *J. Phys. Chem. Solid* **1999**, *60*, 379–384.

(28) Goldys, E. M.; Drozdowica-Tomsia, K.; Sun, J.; Dosev, D.; Kennedy, I. M.; Yatsunenko, S.; Godlewski, M. *J. Am. Chem. Soc.* **2006**, *128*, 14498–14505.

(29) Seo, S. Y.; Sohn, K.-S.; Park, H. D.; Lee, S. *J. Electrochem. Soc.* **2002**, *149*, H12–H18.

showed the characteristic Eu^{3+} 4f-4f emission through the energy transfer from Gd^{3+} to Eu^{3+} and the self-excitation of Eu^{3+}. Cubic $(Eu_xGd_{1-x})_2O_3$ crystallites retaining the original platelet morphology were obtained by annealing the hydroxide samples at 800−1000 °C, which exhibited greatly enhanced photoluminescence properties. The optimal photoluminescence properties of $(Eu_xGd_{1-x})_2O_3$ crystallites were obtained at the Eu^{3+} content of 0.05 and calcination temperature at 1000 °C. The emission intensity of this sample was comparable with that of commercial Y_2O_3:Eu phosphor powder. Higher calcination temperature at 1400−1500 °C yielded monoclinic $(Eu_xGd_{1-x})_2O_3$ crystallites, losing the platelet morphology.

In the present work, we developed a series of layered rare-earth hydroxide solid solutions and the transformed $(Eu_xGd_{1-x})_2O_3$ platelet crystallites, and revealed the dependence of photoluminescence properties on the Eu^{3+} content in this system. The layered hydroxide solid solutions, which offer both anion-exchangeability and photoluminescence properties, may have a wide range of potential applications. Furthermore, the as-transformed cubic $(Eu_xGd_{1-x})_2O_3$ platelet crystallites are promising phosphor materials for optical film devices because of their platelet morphology and excellent photoluminescence properties. This quasi-topotactic transformation approach to produce oxide phosphors may be extended to develop other rare-earth oxide platelet crystallites, such as Y_2O_3:Eu and Gd_2O_3:Tb.

Acknowledgment. This work was supported by CREST of the Japan Science and Technology Agency (JST) and the World Premier International Center (WPI) Initiative on Materials Nanoarchitectonics, MEXT, Japan.

Supporting Information Available: Complete XRD pattern and SEM image of the rare-earth hydroxide solid solutions; TGA curves and photoluminescence properties of the commercial Y_2O_3:Eu phosphor powder. This material is available free of charge via the Internet at http://pubs.acs.org.